

Constraints on f_{NL} and g_{NL} from the analysis of the N-pdf of the CMB large scale anisotropies

P. Vielva¹, J. L. Sanz¹

¹*Instituto de Física de Cantabria (CSIC - Univ. de Cantabria), Avda. Los Castros s/n, 39005 - Santander, Spain*
E-mails : vielva@ifca.unican.es, sanz@ifca.unican.es

Accepted ????. Received ???; in original form 8 June 2022

ABSTRACT

In this paper we extend a previous work (Vielva & Sanz 2009) where we presented a method based on the N-point probability distribution (pdf) to study the Gaussianity of the cosmic microwave background (CMB). We explore a local non-linear perturbative model up to third order as a general characterization of the CMB anisotropies. We focus our analysis in large scale anisotropies ($\theta > 1^\circ$). At these angular scales (the Sachs-Wolfe regime), the non-Gaussian description proposed in this work defaults (under certain conditions) to an approximated local form of the weak non-linear coupling inflationary model. In particular, the *quadratic* and *cubic* terms are governed by the non-linear coupling parameters f_{NL} and g_{NL} , respectively. The extension proposed in this paper allows us to directly constrain these non-linear parameters. Applying the proposed methodology to WMAP 5-yr data, we obtain $-5.6 \times 10^5 < g_{\text{NL}} < 6.4 \times 10^5$, at 95% CL. This result is in agreement with previous findings obtained for equivalent non-Gaussian models and with different non-Gaussian estimators, although this is the first direct constrain on g_{NL} from CMB data. A model selection test is performed, indicating that a Gaussian model (i.e. $f_{\text{NL}} \equiv 0$ and $g_{\text{NL}} \equiv 0$) is preferred to the non-Gaussian scenario. When comparing different non-Gaussian models, we observe that a pure f_{NL} model (i.e. $g_{\text{NL}} \equiv 0$) is the most favoured case, and that a pure g_{NL} model (i.e. $f_{\text{NL}} \equiv 0$) is more likely than a general non-Gaussian scenario (i.e. $f_{\text{NL}} \neq 0$ and $g_{\text{NL}} \neq 0$). Finally, we have analyzed the WMAP data in two independent hemispheres, in particular the ones defined by the dipolar pattern found by Hoftuft et al. (2009). We show that, whereas the g_{NL} value is compatible between both hemispheres, it is not the case for f_{NL} (with a p-value ≈ 0.04). However, if, as suggested by Hoftuft et al. (2009), anisotropy of the data is assumed, the distance between the likelihood distributions for each hemisphere is larger than expected from Gaussian and anisotropic simulations, not only for f_{NL} , but also for g_{NL} (with a p-value of ≈ 0.001 in the case of this latter parameter). This result is an extra evidence for the CMB asymmetries previously reported in WMAP data.

Key words: cosmology: observations – cosmology: cosmic microwave background – methods: data analysis – methods: statistical

1 INTRODUCTION

Current observations of the Cosmic Microwave Background (CMB) temperature and polarization fluctuations, in addition to other astronomical data sets (e.g. Komatsu et al. 2009; Gupta et al. 2009, see Barreiro 2009 for a recent review), provide an overall picture for the origin, evolution, and matter and energy content of the universe, which is usually referred to as the *standard cosmological model*. In this context, we believe the universe to be highly homogeneous and isotropic, in expansion, well described by a Friedmann-

Robertson-Walker metric and with a trivial topology. The space geometry is very close to flat, and it is filled with cold dark matter (CDM) and dark energy (in the form of a cosmological constant, Λ), in addition to baryonic matter and electromagnetic radiation. Large scale structure (LSS) is assumed to be formed by the gravitational collapse of an initially smooth distribution of adiabatic matter fluctuations, which were seeded by initial Gaussian quantum fluctuations generated in a very early inflationary stage of the universe evolution.

It is interesting to mention that, besides the success of

current high quality CMB data (in particular the data provided by the WMAP satellite Hinshaw et al. 2009) in constraining the cosmological parameters with good accuracy and in showing the high degree of homogeneity and isotropy of the Universe (as predicted by the standard inflation scenario, see for instance Liddle & Lyth 2000), it has been, precisely, through the analysis of this very same data, that the CMB community has been allowed to probe fundamental principles and assumptions of the *standard cosmological model*. Most notably, the application of sophisticated statistical analysis to CMB data might help us to understand whether the temperature fluctuations of the primordial radiation are compatible with the fundamental isotropic and Gaussian standard predictions from the *inflationary phase*.

Indeed, the interest of the cosmology community in this field has experienced a significant growth, since several analyses of the WMAP data have reported some hints for departure from isotropy and Gaussianity of the CMB temperature distribution. The literature on the subject is very large, and is still growing, which makes really difficult to provide a complete and updated list of publications. We refer to our previous work (Vielva & Sanz 2009) for an (almost) complete review.

Among the previously mentioned analyses, those related to the study of non-standard inflationary models have attracted a larger attention. For instance, the non-linear coupling parameter f_{NL} that describes the non-linear evolution of the inflationary potential (see e.g. Bartolo et al. 2004, and references therein) has been constrained by several groups, from the analysis of the WMAP data: using the angular bispectrum (Komatsu et al. 2003; Creminelli et al. 2007; Spergel et al. 2007; Komatsu et al. 2009; Yadav & Wandelt 2008; Smith et al. 2009); applying the Minkowski functionals (Komatsu et al. 2003; Spergel et al. 2007; Gott et al. 2007; Hikage et al. 2008; Komatsu et al. 2009); using different statistics based on wavelets (Mukherjee & Wang 2004; Cabella et al. 2005; Curto et al. 2009a,b; Pietrobon et al. 2009; Rudjord et al. 2009), and by exploring the N-pdf (Vielva & Sanz 2009). Besides marginal detections of $f_{\text{NL}} > 0$ (with a probability of around 95%, Yadav & Wandelt 2008; Rudjord et al. 2009), there is a general consensus on the WMAP compatibility with the predictions made by the standard inflationary scenario at least at 95% confidence level. The current best limits obtained from the CMB data are: $-4 < f_{\text{NL}} < 80$ at 95% CL by Smith et al. (2009). In addition, very recently, promising constraints coming out from the analysis of LSS have been reported: $-29 < f_{\text{NL}} < 70$ at 95% CL (Slozar et al. 2008).

The aim of this paper is to extend our previous work (Vielva & Sanz 2009), where the full N-pdf of a non-Gaussian model that describes the CMB anisotropies as a local (pixel-by-pixel) non-linear expansion of the temperature fluctuations (up to second order) was derived. For this model—that, at large scales, can be considered as an approximation to the weak non-linear coupling scenario—we are able to build the exact likelihood on pixel space. Working in pixel space allows one to include easily non-ideal observational conditions, like incomplete sky coverage and anisotropic noise. The extension of the present work is to account for higher order moments in the expansion, in particular, we are able to directly obtain constraints on g_{NL} ,

that is the coupling parameter governing the cubic term of the weak non-linear expansion.

As far as we are aware, direct constraints on g_{NL} have been made available only very recently (Desjacques & Seljak 2009) and are obtained from LSS analyses: $-3.5 \times 10^5 < g_{\text{NL}} < 8.2 \times 10^5$ at 95% CL. This constraint was obtained for the specific case in which the coupling parameter governing the quadratic term (f_{NL}) is negligible (i.e. $f_{\text{NL}} \equiv 0$, which is the situation required for some curvaton inflationary models, e.g. Sasaki et al. 2006; Enqvist & Takahashi 2008; Huang 2009). We present in this work the first direct measurement of g_{NL} obtained from CMB data. In addition to study the particular case of $f_{\text{NL}} \equiv 0$, we also consider a more general case in which a joint estimation of f_{NL} and g_{NL} is performed. Finally, and justified by recent findings (e.g., Hoftuft et al. 2009), we compute the N-pdf in two different hemispheres, and derive from it constraints on f_{NL} and g_{NL} for this hemispherical division of the celestial sphere.

The paper is organized as follows. In Section 2 we describe the physical model based on the local expansion of the CMB fluctuations and derive the full posterior probability, recalling how it defaults to the case already addressed in Vielva & Sanz (2009). In Section 3 we check the methodology against WMAP-like simulations. Results on WMAP 5-year data are presented in Section 4. Conclusions are given in Section 5. Finally, in Appendix A, we provide a detailed computation of the full N-pdf.

2 THE NON-GAUSSIAN MODEL

Although current CMB measurements are well described by random Gaussian anisotropies (as it is predicted by the standard inflationary scenario), observations also allows for small departures from Gaussianity, that could indicate the presence of an underlying physical process generated in non-standard models.

As we did in Vielva & Sanz (2009) we adopt a parametric non-Gaussian model for the CMB anisotropies, that accounts for a small and local (i.e. point-to-point) perturbation of the CMB temperature fluctuations, around its intrinsic Gaussian distribution:

$$\begin{aligned} \Delta T_i &= (\Delta T_i)_G + a [(\Delta T_i)_G^2 - \langle (\Delta T_i)_G^2 \rangle] + \\ & b (\Delta T_i)_G^3 + \mathcal{O}((\Delta T_i)_G^4). \end{aligned} \quad (1)$$

The *linear term* $(\Delta T_i)_G$ is given by a Gaussian N-point probability density function (N-pdf) that is easily described in terms of the standard inflationary model. The second and third terms on the right-hand side are the *quadratic* and the *cubic* perturbation terms, respectively, and they are governed by the a and b parameters.

The sub-index i refers to a given direction in the sky that, in practice, is described in terms of a certain pixelization of the sphere. The operator $\langle \cdot \rangle$ indicates averaging over all the pixels defining the sky coverage. We have not considered explicitly an *instrumental noise*-like term, since, for the particular case that we intend to explore (i.e., large-scale CMB data), its contribution to the measured signal (for experiments like WMAP or Planck) is negligible. Precisely at the large-scale regime, the term ΔT_i is mostly dominated by the Sachs-Wolfe contribution to the CMB fluctuations,

and can be related to the primordial gravitational potential Φ (e.g. Komatsu et al. 2001) by:

$$\Delta T_i \approx -\frac{T_0}{3} \Phi_i, \quad (2)$$

where T_0 is the CMB temperature. Small departures from Gaussianity of the Φ potential are usually described via the weak non-linear coupling model:

$$\Phi_i = \Phi_{L,i} + f_{\text{NL}} (\Phi_{L,i}^2 - \langle \Phi_{L,i}^2 \rangle) + g_{\text{NL}} \Phi_{L,i}^3 + \mathcal{O}(\Phi_{L,i}^4). \quad (3)$$

Taking into account equations 1, 2 and 3, and always considering the specific case for scales larger than the horizon scale at the recombination time (i.e. above the degree scale), it is trivial to establish the following relations:

$$f_{\text{NL}} \cong -\frac{T_0}{3} a, \quad g_{\text{NL}} \cong \left(\frac{T_0}{3}\right)^2 b. \quad (4)$$

At this point, it is worth mentioning that the model in equation 1 does not pretend to incorporate all the gravitational and non-gravitational effects, due to the evolution of the initial quadratic potential model, but rather allows for a useful parametrization for describing a small departure from Gaussianity. The relationships in equation 4 have to be understood just as an asymptotic equivalence for large scales.

Let us simplify the notation by transforming the Gaussian term $(\Delta T_i)_G$ into a zero mean and unit variance random variable ϕ_i . It is easy to show that equation 1 transforms into:

$$x_i = \phi_i + a\sigma(\phi_i^2 - 1) + b\sigma^2\phi_i^3 + \mathcal{O}(\sigma^3) \quad (5)$$

where:

$$x \equiv \frac{1}{\sigma} \Delta T, \quad \phi \equiv \frac{1}{\sigma} (\Delta T)_G \quad (6)$$

and $\sigma^2 \equiv \langle (\Delta T_i)_G^2 \rangle$ is the standard deviation of the CMB fluctuations. Trivially, the normalized Gaussian variable ϕ satisfies:

$$\begin{aligned} \langle \phi_i^{2n+1} \rangle &= 0 \\ \langle \phi_i^{2m} \rangle &= (2m-1)!! \\ \langle \phi_i \phi_j \rangle &= \xi_{ij}, \end{aligned} \quad (7)$$

where $n \geq 0$ and $m > 0$ are integer numbers, and ξ_{ij} represents the normalized correlation between pixels i and j . Obviously, the N-pdf of the $\phi = \{\phi_1, \phi_2, \dots, \phi_N\}$ random field (where N refers to the number of pixels on the sphere that are actually observed) is given by a multivariate Gaussian distribution:

$$p(\phi) = \frac{1}{(2\pi)^{N/2} (\det \xi)^{1/2}} e^{-\frac{1}{2} \phi \xi^{-1} \phi^t}, \quad (8)$$

where ξ denotes the correlation matrix and operator \cdot^t denotes standard matrix/vector transpose.

As it was the case in Vielva & Sanz (2009), the objective is to obtain the N-pdf associated to the non-Gaussian $\mathbf{x} = \{x_1, x_2, \dots, x_N\}$ field, as a function of the non-linear coupling parameters (or, equivalently, the a and b coefficients):

$$p(\mathbf{x}|a, b) = p(\phi = \phi(\mathbf{x}))Z. \quad (9)$$

In this expression, Z is the determinant of the Jacobian for the $\phi \rightarrow \mathbf{x}$ transformation. Because the proposed model

is local (i.e. point-to-point), the Jacobian matrix is diagonal and, therefore, Z is given by:

$$Z = \det \left[\frac{\partial \phi_i}{\partial x_j} \right] = \prod_i \left(\frac{\partial \phi_i}{\partial x_i} \right). \quad (10)$$

Both, equations 9 and 10, require the inversion of equation 5: i.e., to express ϕ_i as a function of x_i . After some algebra, it can be proved that:

$$\phi_i = x_i + \eta_i \sigma + \nu_i \sigma^2 + \lambda_i \sigma^3 + \mu_i \sigma^4 + \mathcal{O}(\sigma^5), \quad (11)$$

where:

$$\begin{aligned} \eta_i &= -a(x_i^2 - 1) \\ \nu_i &= (2a^2 - b)x_i^3 - 2a^2 x_i \\ \lambda_i &= (5ab - 5a^3)x_i^4 + (6a^3 - 3ab)x_i^2 - a^3 \\ \mu_i &= (14a^4 - 21a^2 b + 3b^2)x_i^5 + (-20a^4 + 20a^2 b)x_i^3 \\ &\quad + (6a^4 - 3a^2 b)x_i. \end{aligned} \quad (12)$$

Instead of dealing with $p(\mathbf{x}|a, b)$, it is equivalent, but more convenient, to work with the log-likelihood $\mathcal{L}(\mathbf{x}|a, b)$:

$$\mathcal{L}(\mathbf{x}|a, b) = \log \frac{p(\mathbf{x}|a, b)}{p(\mathbf{x}|0)}. \quad (13)$$

A detailed computation of $\mathcal{L}(\mathbf{x}|a, b)$ is given in Appendix A. Let us just recall here its final expression:

$$\begin{aligned} \frac{1}{N} \mathcal{L}(\mathbf{x}|a, b) &= F\sigma + (2a^2 - 3b + G)\sigma^2 + H\sigma^3 \\ &\quad + \left(12a^4 - 36a^2 b + \frac{27}{2}b^2 + I\right)\sigma^4, \end{aligned} \quad (14)$$

where N is the number of data points, and F, G, H and I are functions of a and b (see A13). The desired N-pdf, $p(\mathbf{x}|a, b)$ is obtained by the inversion of equation 13, and taking into account that $p(\mathbf{x}|0) \equiv p(\phi = x)$, i.e., the known Gaussian N-pdf in equation 8.

3 APPLICATION TO WMAP SIMULATIONS

In this Section we aim to investigate the performance of the parameters estimation from the N-pdf derived in the previous Section. We explore different non-Gaussian scenarios; in particular, we study three particular cases of special interest:

- *Case i*) $a \neq 0, b = 0$. This scenario would correspond, for example, to the case for the slow-roll standard inflation
- *Case ii*) $a = 0, b \neq 0$. This scenario would correspond to the particular situation for some curvaton models.
- *Case iii*) $a \neq 0, b \neq 0$. It is a generic case, not representing any specific inflationary model, but rather a general scenario.

In particular, we will study how the determination of the parameters governing the non-Gaussian terms is performed, and what is the impact when one is exploring different configurations. In the next subsections, we will focus, first, in the case in which a slow-roll standard like scenario is assumed (i.e., we only try to adjust for the *quadratic* term, assuming the *cubic* one is negligible), whatever the data is actually a pure *quadratic* or *cubic* model, or a general non-Gaussian scenario. Second, we will follow a similar analysis, but assuming the estimation of a pure *cubic* term. Finally, we will address the case for a joint estimation of both

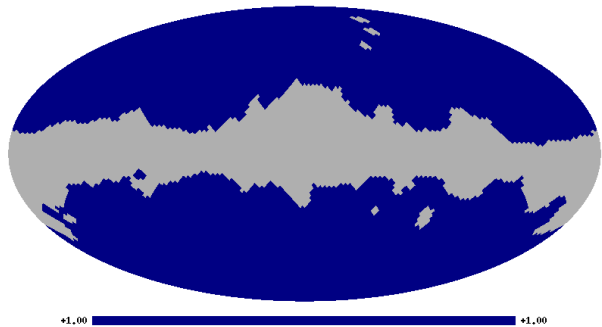


Figure 1. Mask at NSIDE=32 HEALPix resolution used in this work. It corresponds to the WMAP KQ75 mask, although the point source masking has not been considered, since the point like-emission due to extragalactic sources is negligible at the considered resolution. At this pixel resolution, the mask keeps around 69% of the sky.

(*quadratic* and *cubic*) terms. In the following, we will refer all our results in terms of the non-linear coupling parameters (f_{NL} and g_{NL}), rather than to the a and b coefficients.

In order to carry out this analysis, we have generated Gaussian CMB simulations coherent with the model induced from the WMAP 5-year data at NSIDE=32 HEALPix (Górski et al. 2005) resolution ($\approx 2^\circ$).

The procedure to generate a CMB Gaussian simulation $-(\Delta T)_G$ in equation 1— is as follows. First, we simulate WMAP observations for the Q1, Q2, V1, V2, W1, W2, W3, W4 difference assemblies at NSIDE=512 HEALPix resolution. The C_ℓ obtained with the cosmological parameters provided by the best-fit to WMAP data alone (Table 6 in Hinshaw et al. 2009), are assumed.

Second, a single co-added CMB map is computed afterwards through a noise-weighted linear combination of the eight maps (from Q1 to W4). The weights used in this linear combination are proportional to the inverse mean noise variance provided by the WMAP team. They are independent on the position (i.e., they are uniform across the sky for a given difference assembly) and they are forced to be normalized to unity. Notice that we have not added Gaussian white noise to the different difference assembly maps, since we have already checked that instrumental noise plays a negligible role at the angular resolution in which we are interested ($\approx 2^\circ$, see Vielva & Sanz 2009, for details).

Third, the co-added map at NSIDE=512 is degraded down to the final resolution of NSIDE=32, and a mask representing a sky coverage like the one allowed by the WMAP KQ75 mask (Gold et al. 2009) is adopted. At NSIDE=32 the mask keeps around 69% of the sky. The mask is given in figure 1. Let us remark that observational constraints from an incomplete sky coverage can be easily taken into account by the local non-Gaussian model proposed in this work, since it is naturally defined in pixel space. This is not the case for other common estimators like the bispectrum, where the presence of an incomplete sky coverage is usually translated into a loss of efficiency.

We have generated 500000 simulations of $(\Delta T)_G$, computed as described above, to estimate the correlation matrix ξ accounting for the Gaussian CMB cross-correlations. We have checked that this large number of simulations is enough

to obtain an accurate description of the CMB Gaussian fluctuations.

In addition, we have generated another set of 1000 simulations. These are required to carry out the statistical analysis to check the performance of the parameter estimation. Each one of these 1000 $(\Delta T)_G$ simulations are transformed into \mathbf{x} (following equations 1 and 6) to study the response of the statistical tools as a function of the non-linear parameters defining the local non-Gaussian model proposed in equation 5.

Finally, let us remark that hereinafter the likelihood maximization is simply performed by exploring a grid of values in the parameter space of the non-linear coupling parameters. The step used in the grid is small enough to guarantee a good estimation both of the likelihood peak and tails.

3.1 The recovery of f_{NL} in the presence of a *cubic* term

The results obtained from the 1000 simulations are given in figure 2. We have explored 16 different non-Gaussian models, accounting for all the possible combinations obtained with simulated \bar{g}_{NL} values of 0, 3×10^5 , 5×10^5 and 10^6 , and \bar{f}_{NL} values of 0, 200, 400 and 600. For each panel, we present the histogram of the maximum-likelihood estimation of the non-linear coupling *quadratic* parameter: \hat{f}_{NL} . Notice that we refer to a simulated value of a given non-linear coupling parameter (x_{NL}), as \bar{x}_{NL} , whereas that its estimation via the maximum-likelihood is denoted as \hat{x}_{NL} . Vertical dashed lines in each panel, indicate the value of the maximum-likelihood estimation for the parameter.

As it can be noticed from the figure, when the simulated data satisfies the condition of the particular explored model (i.e., $\bar{g}_{\text{NL}} \equiv 0$, first column), the f_{NL} is accurately and efficiently estimated, at least for values of $\bar{f}_{\text{NL}} < 600$. Actually, this is a result that we already obtained in Vielva & Sanz (2009), which indicates that for $\bar{f}_{\text{NL}} > 600$, the perturbative model stars to be not valid any longer.

However, when the simulated non-Gaussian maps also contain a significant contribution from a *cubic* term, the bias in the determination of the f_{NL} parameter stars to be evident already for lower values of the simulated \bar{f}_{NL} . It is interesting to notice that, even if the simulated \bar{g}_{NL} is large (for instance $\bar{g}_{\text{NL}} = 10^6$), we do not see any significant bias in \hat{f}_{NL} , for simulated \bar{f}_{NL} values lower than 200.

Summarizing, we can infer that for non-Gaussian scenarios with $|\bar{f}_{\text{NL}}| \lesssim 400$ and $|\bar{g}_{\text{NL}}| \lesssim 5 \times 10^5$, no significant bias on the estimation of a pure *quadratic* term is found. It is worth mentioning that these range of values are in agreement with predictions from most of the physically motivated non-Gaussian inflationary models. Notice that, in general, even for the cases in which a bias is observed, the efficiency in the determination of f_{NL} (somehow related to the width of the histograms) is almost unaltered.

3.2 The recovery of g_{NL} in the presence of a *quadratic* term

As for the previous case, a graphical representation of the results obtained from the 1000 simulations is given in figure 3. We have explored the same 16 different non-Gaussian

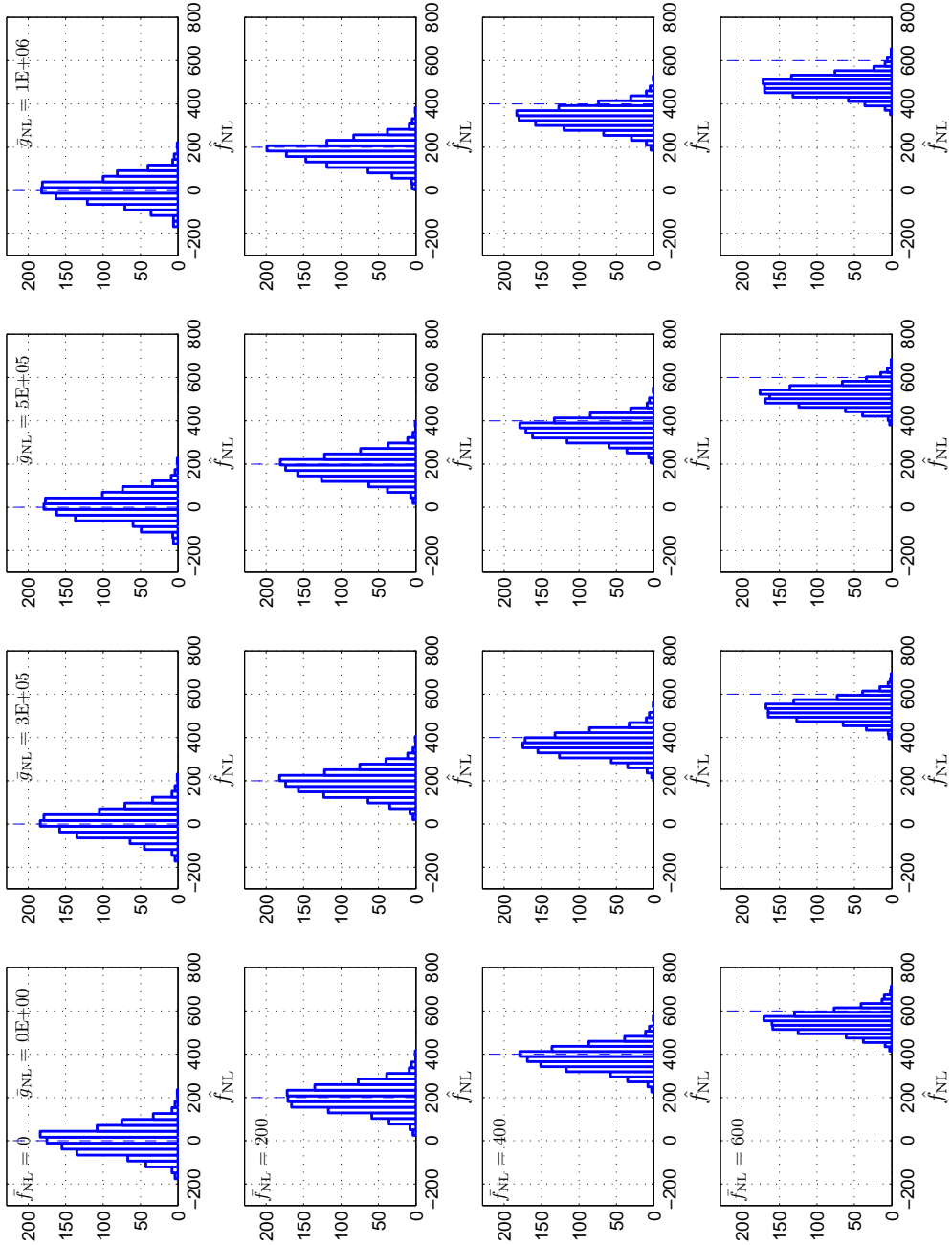


Figure 2. These panels represent the accuracy and efficiency on the estimation of the f_{NL} parameter. From left to right, the columns correspond to simulated \bar{g}_{NL} values of: 0 , 3×10^5 , 5×10^5 and 10^6 . Similarly, from top to bottom, rows correspond to simulated \bar{f}_{NL} values of: 0 , 200 , 400 and 600 . The histograms show the distribution of the obtained values of \hat{f}_{NL} for each case. The vertical dashed lines indicate the simulated \bar{f}_{NL} value, and help to identify the presence of a possible bias.

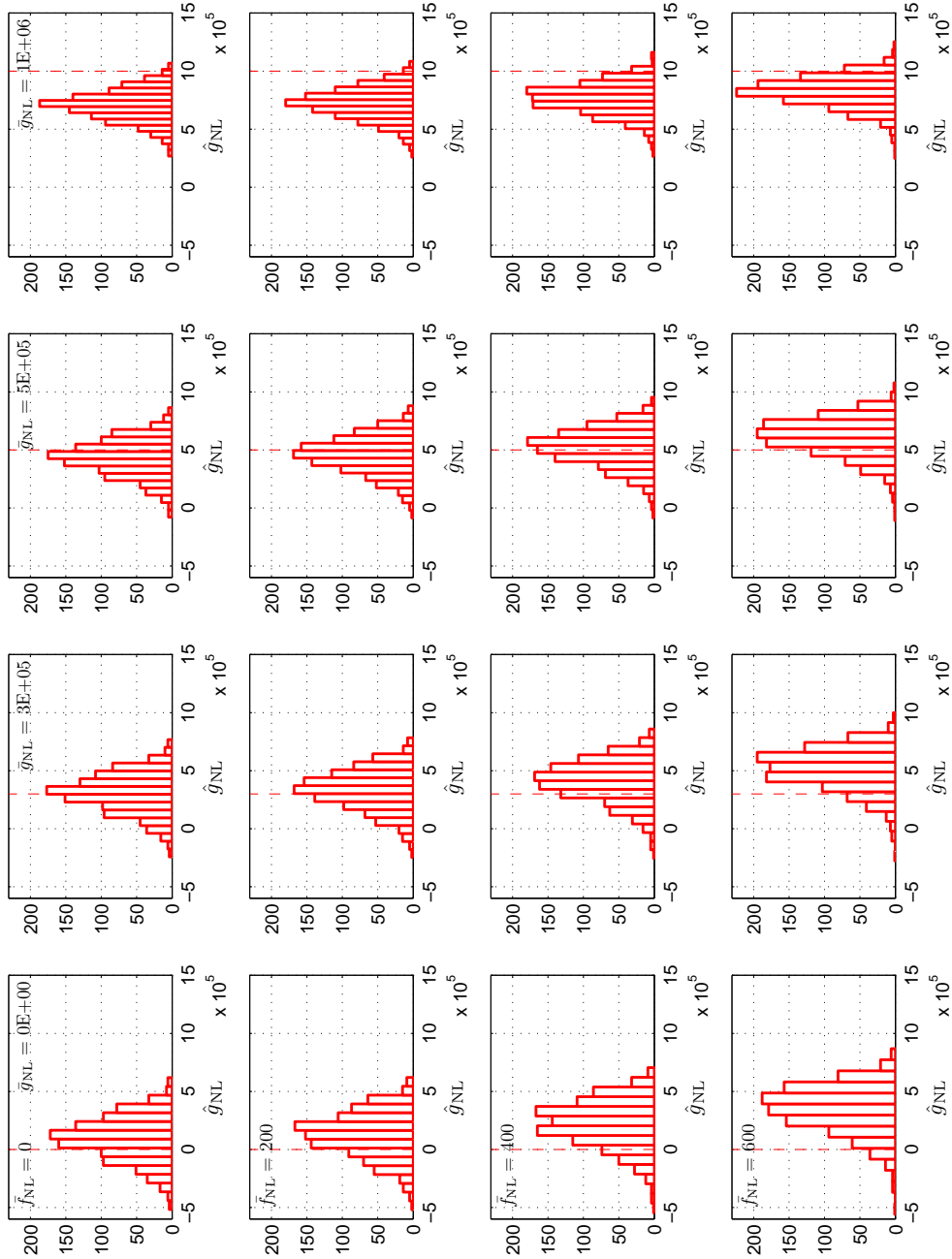


Figure 3. These panels represent the accuracy and efficiency on the estimation of the g_{NL} parameter. From left to right, the columns correspond to simulated \bar{g}_{NL} values of: 0, 3×10^5 , 5×10^5 and 10^6 . Similarly, from top to bottom, rows correspond to simulated \bar{f}_{NL} values of: 0, 200, 400 and 600. The histograms show the distribution of the obtained values of \hat{g}_{NL} for each case. The vertical dashed lines indicate the simulated \bar{g}_{NL} value, and help to identify the presence of a possible bias.

models already described above. As it can be noticed from the figure, when the simulated data corresponds to the explored model (i.e., $\bar{f}_{\text{NL}} \equiv 0$, first row), the g_{NL} parameter is reasonably estimated, at least for simulated $\bar{g}_{\text{NL}} < 10^6$.

However, when the simulated non-Gaussian maps also contain a significant contribution from the *quadratic* term, a bias in the determination of the g_{NL} parameter starts to be notorious for lower values of the simulated \bar{g}_{NL} coefficient. In particular, the plots of the first column (i.e., $\bar{g}_{\text{NL}} \equiv 0$) show a clear bias on \hat{g}_{NL} . This indicates that, when the analyzed case corresponds to a pure *quadratic* scenario, and a pure *cubic* model is assumed, the g_{NL} estimator is sensitive to the *quadratic* non-Gaussianity and, somehow, it absorbs the non-Gaussianity in the form of a fake *cubic* term. In particular, an input value of $\bar{f}_{\text{NL}} \equiv 400$ is determined as a pure $\hat{g}_{\text{NL}} \approx 2.5 \times 10^5$. Notice that this was not the situation for the previous case, where the f_{NL} estimation was not sensitive to the presence of a pure *cubic* model (at least for reasonable values of \bar{g}_{NL}). This is an expected results, since, any skewed distribution would imply the presence of a certain degree of kurtosis, whereas the opposite is not necessary true.

3.3 The general case: the joint recovery of f_{NL} and g_{NL}

Finally, we have also explored the case of a joint estimation of the *quadratic* and *cubic* terms. The results obtained from the 1000 simulations are given in figure 4. As for the previous cases, we have explored the same 16 different non-Gaussian models already described above. The plots represent the contours of the 2-D histograms obtained for the pair $(\hat{f}_{\text{NL}}, \hat{g}_{\text{NL}})$ of the maximum-likelihood estimation. Vertical and horizontal dashed lines indicate the simulated \bar{f}_{NL} and \bar{g}_{NL} values, respectively.

As it can be noticed from the figure, only for the regime $|\bar{f}_{\text{NL}}| \lesssim 400$ and $|\bar{g}_{\text{NL}}| \lesssim 5 \times 10^5$, we obtain an accurate and efficient estimation of the non-linear coupling parameters. As it was reported above, this regime correspond to the boundaries obtained from the pure f_{NL} case.

It is interesting to notice the presence of very large biases for cases outside of the previous range. In particular, estimations tend to move towards a region of the parameter space of larger values of both, f_{NL} and g_{NL} . Only a secondary peak in the 2-D histogram corresponds to the simulated pair of values.

This result, combined with the previous ones, indicates that the non-Gaussian model proposed in equation 1 is only valid up to values of the *quadratic* and *cubic* terms of around 1% and 0.05%, respectively.

4 APPLICATION TO WMAP 5-YEAR DATA

We have studied the compatibility of the WMAP 5-year data with a non-Gaussian model as the one described in equation 1. In particular, we have analyzed the co-added CMB map generated from the global noise-weighted linear combination of the reduced foreground maps for the Q1, Q2, V1, V2, W1, W2, W3 and W4 difference assemblies (see Gold et al. 2009, for details). The weights are proportional

to the inverse average noise variance across the sky, and are normalized to unity. This linear combination is made at NSIDE=512 HEALPix resolution, being degraded afterwards down to NSIDE=32.

Under these circumstances, we are in the same condition as for the analysis performed on the simulations described in Section 3. Therefore, the theoretical multinormal covariance of the CMB temperature fluctuations ($\boldsymbol{\xi}$) is the one already computed with the 500000 simulations (see previous Section).

Two different analysis were performed. The first accounts for an all-sky study (except for the sky regions covered by the Galactic mask described in the previous Section), where constraints on the non-linear coupling parameters from different scenarios are presented. We will present as well results derived from a model selection approach, where we investigate which are the models that are more favoured by the data. The second analysis explores the WMAP data compatibility with the local non-Gaussian model in two different hemispheres. In particular, we have studied independently the two hemispheres related to the dipolar pattern described in Hoftuft et al. (2009).

4.1 All-sky analysis

We have computed the full N-pdf in equation 9, for three different scenarios: a non-Gaussian model with a pure *quadratic* term (i.e., $g_{\text{NL}} \equiv 0$), another case with a pure *cubic* term (i.e., $f_{\text{NL}} \equiv 0$), and a general non-Gaussian model (i.e., $f_{\text{NL}} \neq 0$ and $g_{\text{NL}} \neq 0$),

Results are given in figure 5. Left panel shows the likelihood obtained for the first case: $p(\boldsymbol{x}|f_{\text{NL}})$. Actually, this result is the one that we already obtained in our previous work (Vielva & Sanz 2009). The maximum-likelihood estimation for the *quadratic* factor is $\hat{f}_{\text{NL}} = -32^1$. The constraint on the non-Gaussian parameter is: $-154 < f_{\text{NL}} < 94$ at 95%.

The middle panel in figure 5 presents the likelihood obtained from a model with a pure *cubic* term: $p(\boldsymbol{x}|g_{\text{NL}})$. The maximum-likelihood estimation for the *quadratic* factor is $\hat{g}_{\text{NL}} = 42785$. The constraint on the parameter is: $-5.6 \times 10^5 < g_{\text{NL}} < 6.4 \times 10^5$ at 95%. This result is compatible with a previous finding obtained from the analysis of LSS data (Desjacques & Seljak 2009). The result reported in this work is, as far as we know, the first direct constraint of g_{NL} from CMB data alone.

The right panel in figure 5 shows the contour levels at the 68%, 95% and 99% CL, for the likelihood obtained from an analysis of a general *quadratic* and *cubic* model: $p(\boldsymbol{x}|f_{\text{NL}}, g_{\text{NL}})$. Notice that the maximum likelihood estimation for the f_{NL} and g_{NL} parameters are similar to those obtained from the previous cases (where the pure models were investigated). Even more, the marginalized distributions for the two parameters are extremely similar to the likelihood distributions discussed previously, and, therefore,

¹ Notice that in Vielva & Sanz (2009) we used a different definition between the primordial gravitational potential Φ and the CMB temperature. This difference implies that, in our previous work, the f_{NL} parameter had an opposite sign with respect to the definition used in this paper.

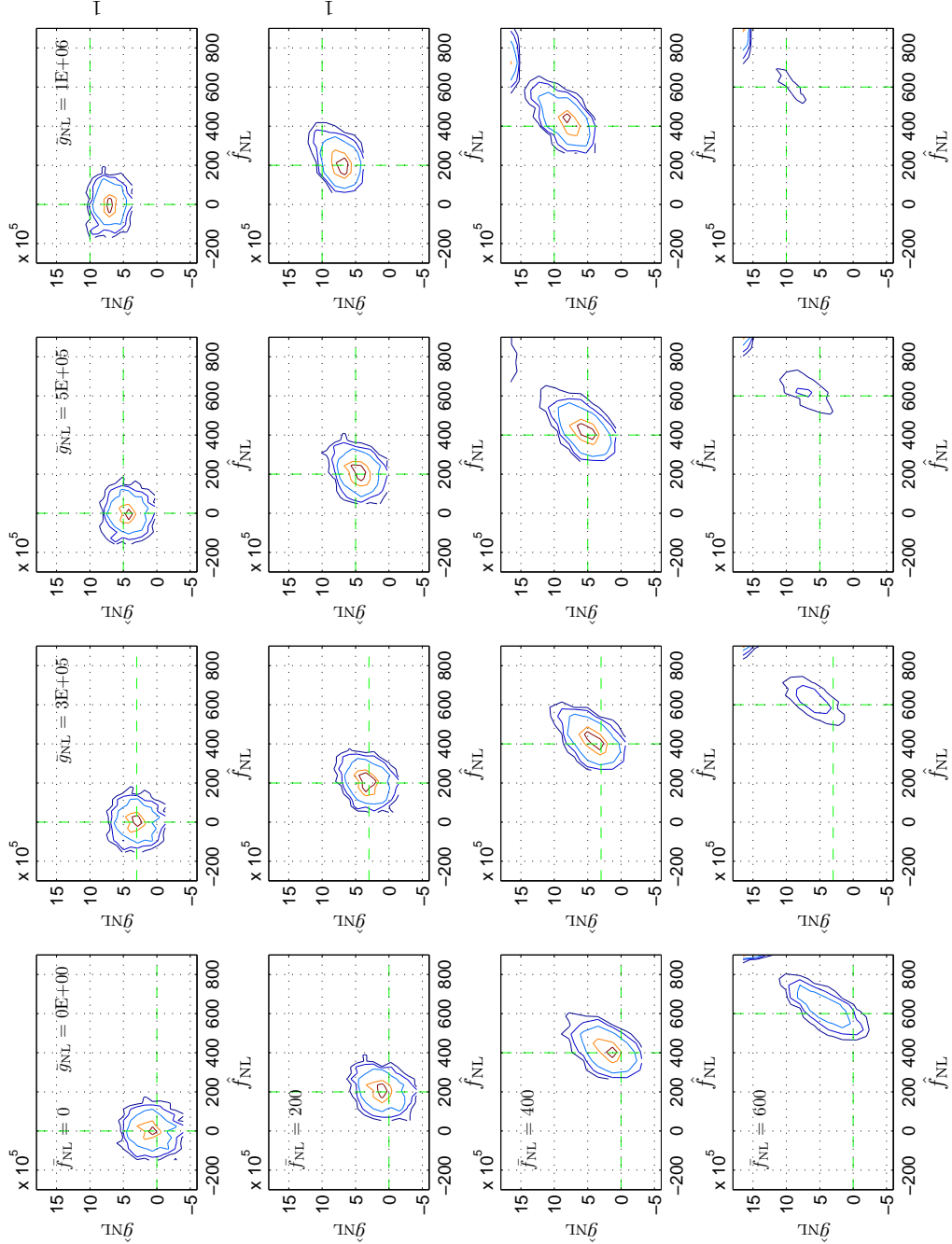


Figure 4. These panels represent the accuracy and efficiency on the joint estimation of the f_{NL} and g_{NL} parameters. From left to right, the columns correspond to simulated \bar{g}_{NL} values of: 0, 3×10^5 , 5×10^5 and 10^6 . Similarly, from top to bottom, rows correspond to simulated \bar{f}_{NL} values of: 0, 200, 400 and 600. The contours show the distribution of the obtained values of the pair $(\hat{f}_{\text{NL}}, \hat{g}_{\text{NL}})$ for each case. The vertical and horizontal dashed lines indicate the simulated \bar{f}_{NL} and \bar{g}_{NL} values, respectively, and help to identify the presence of a possible bias.

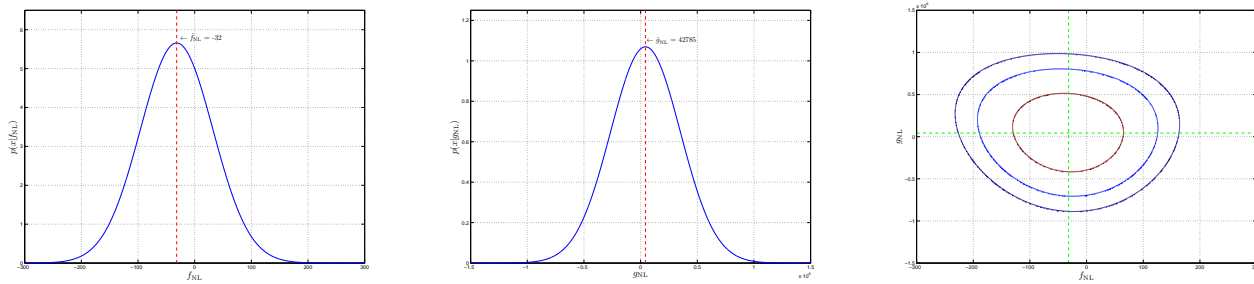


Figure 5. Likelihood distribution of the non-linear parameters obtained by analyzing 1000 simulations, according to the local non-Gaussian model given in equation 1. Left panel correspond to a pure f_{NL} analysis: $p(\mathbf{x}|f_{\text{NL}})$. Middle plot shows the result for a pure g_{NL} model: $p(\mathbf{x}|g_{\text{NL}})$. Right panel provides the 68%, 95% and 99% contour levels of the likelihood obtained from a joint f_{NL} , g_{NL} analysis of the WMAP 5-year data: $p(\mathbf{x}|f_{\text{NL}}, g_{\text{NL}})$.

the constraints on the non-linear coupling parameters are virtually the same.

Finally, we want to comment a few words about two issues: the incorporation of possible *a priori* information related to the parameters defining the non-Gaussian model, and the application of model selection criteria (or hypothesis tests) to discriminate among the Gaussian model and different non-Gaussian models.

As we largely discussed in our previous work (Vielva & Sanz 2009), one of the major advantages of computing the full N-pdf on the non-Gaussian model is that, in addition to provide a maximum-likelihood estimation for the non-linear coupling parameters, we have a full description of the statistical properties of the problem. More in particular, if we could have any physical (or empirical) motivated prior for the f_{NL} and g_{NL} parameters, it could be used together with the likelihood function to perform a full Bayesian parameter estimation. This aspect has not been considered in this work, precisely because such a well motivated prior is lacking. Actually, a possible and trivial *a priori* information that could be used in this specific case, would be to limit the range of values that can be taken by f_{NL} and g_{NL} , such as the non-Gaussian model is, indeed, a local perturbation of a Gaussian field (i.e., the typical values that we discussed in Section 3). However, these priors do not seem to be quite useful since, first, we do not have any evidence to chose any different form for the prior that an uniform value over the parameters range; and, second, the limits of these ranges are somehow arbitrary. These kind of priors do not provide any further knowledge on the Bayesian parameter determination: as it is well known, such estimation would be totally driven by the likelihood itself, since it is fully defined within any reasonable *a priori* ranges.

The possibility of performing a model selection approach is an extra advantage of dealing with the full N-pdf. Of course, under the presence of an hypothetical well motivated prior on the non-linear coupling parameters, model selection could be done in terms of the Bayesian evidence or the ratio of posterior probabilities (see Vielva & Sanz 2009, for a specific discussion on this application). However, the lack of such a prior (as we discussed above), makes the application of a full Bayesian model selection framework significantly less powerful than in other situations: as it is very well known, the use of uniform priors for all the parameters would provide very little information, since the results would

be very much dependent on the size of the parameters range. Despite this, we can still make a worthy use of the likelihood to perform model selection. In particular, some asymptotic model selection criteria, like the *Akaike Information Criteria* (AIC, Akaike 1973) and the *Bayesian Information Criteria* (BIC, Schwarz 1978), can be applied. Both methods provide a ranging index for competitive hypotheses, where the most likely one is indicated by the lowest value of the index. The AIC and BIC indices depend on the maximum value of the log-likelihood ($\max[\mathcal{L}(\mathbf{x}|\Theta)] \equiv \hat{\mathcal{L}}$):

$$\text{AIC}(H_i) = 2(p - \hat{\mathcal{L}}),$$

$$\text{BIC}(H_i) = 2\left(\frac{p}{2} \log N - \hat{\mathcal{L}}\right),$$

where p is the number of parameters that determine the hypothesis or model H_i . We have applied these two asymptotic model selection criteria to the WMAP 5-year data. Defining the Gaussian model as H_0 , the pure *quadratic* model as H_1 , the pure *cubic* model as H_2 , and the general non-Gaussian model as H_3 , and considering the maximum value for the log-likelihoods obtained for all these cases, we obtain: $\text{AIC}(H_0) < \text{AIC}(H_1) < \text{AIC}(H_2) < \text{AIC}(H_3)$, and $\text{BIC}(H_0) < \text{BIC}(H_1) < \text{BIC}(H_2) < \text{BIC}(H_3)$. That is, the most likely model is the Gaussian one (what is in agreement with the results obtained from the parameter determination, since $f_{\text{NL}} \equiv 0$ and $g_{\text{NL}} \equiv 0$ can not be rejected at any meaningful confidence level). Among the non-Gaussian models, a pure f_{NL} model is the most likely scenario, being a joint f_{NL} , g_{NL} model the most disfavoured by the WMAP 5-year data.

4.2 Hemispherical analysis

Among the large number of the WMAP *anomalies* that have been reported in the literature, an anisotropy manifested in the form of a hemispherical asymmetry is one of the topics that has been more largely studied (e.g., Eriksen et al. 2004a; Hansen et al. 2004b). Most of the works related to this issue, have reported that such asymmetry is more marked for a north-south hemispherical division relatively close to the Northern and Southern Ecliptic hemispheres.

In a recent work, Hoftuft et al. (2009) reported that large scale WMAP data was compatible with such kind of anisotropy, in the form of a dipolar modulation defined by a preferred direction pointing toward the Galactic coordinates $(l, b) = (224^\circ, -22^\circ)$.

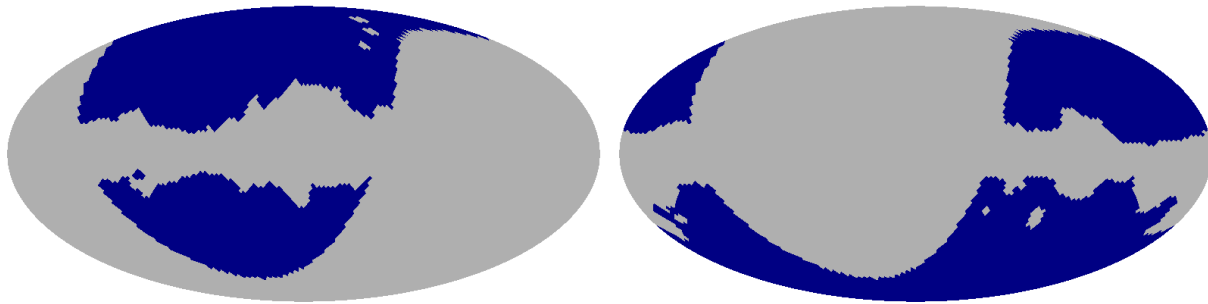


Figure 6. These plots show the areas of the sky that are independently analyzed. The panel on the left accounts for the sky that, being allowed by the Galactic mask (see Section 3), corresponds to the *Northern hemisphere* of the sky division considered in this work. Equivalently, the right panel presents the region of the sky that is analyzed when the *Southern hemisphere* is addressed.

Motivated by these results, we have repeated the analysis described in the previous subsection, but addressing independently the two hemispheres associated to the dipolar pattern found by Hoftuft et al. (2009). Hereinafter, we will refer to the *Northern hemisphere* of this dipolar pattern, as the half the of celestial sphere whose pole is closer to the Northern Ecliptic Pole, and, equivalently, we will indicate as the *Southern hemisphere* the complementary half of the sky. The corresponding areas of the sky that are analyzed are shown in figure 6. The left and right panels show the allowed sky regions, when the *Northern* and *Southern hemispheres* of the dipolar pattern are independently addressed, respectively. Notice that the regions not allowed by the Galactic mask are also excluded from the analysis. The portion of the sky that is analyzed is around 34% for the *Northern hemisphere*, and around 35% for the *Southern* half.

As we discussed in the previous subsection, the constraints of the f_{NL} and g_{NL} parameters obtained from the analysis of pure *quadratic* and *cubic* non-Gaussian models, do not differ significantly from those obtained from a general analysis of a joint scenario. This is expected for a regime of relatively low values of the non-linear coupling parameters. For that reason, in the present study we will only consider the following two cases: a pure *quadratic* (i.e. $g_{\text{NL}} \equiv 0$) and a pure *cubic* (i.e. $f_{\text{NL}} \equiv 0$) models. Results are given in figure 7. We present the likelihood probabilities for the first case $-p(\mathbf{x}|f_{\text{NL}})$ — in the left plot, and the one corresponding to the second case $-p(\mathbf{x}|g_{\text{NL}})$ — in the right panel. Each plot shows the results for the *Northern* (dashed lines), and the *Southern* (dot-dashed lines) hemispheres. The maximum likelihood estimation for the non-linear coupling parameters are given as vertical lines.

The right panel shows that both hemisphere have a similar likelihood ($p(\mathbf{x}|g_{\text{NL}})$) for the case of a pure *cubic* model. However, interestingly, it is not the case when addressing a $g_{\text{NL}} \equiv 0$ scenario. In this case, we notice two important results. First, whereas the f_{NL} estimation from the analysis of the *Northern hemisphere* provides a constraint compatible with the Gaussian scenario, it is not the case for the *Southern hemisphere*. In fact, we find that $f_{\text{NL}} < 0$ at 96% CL. In particular we find: $\hat{f}_{\text{NL}} = -164 \pm 62$. Second, the distance between both distributions is too large. Let us make use of the Kullback–Leibler divergence (KLD, Kullback & Leibler 1951) as a measurement of the distance between the two

likelihoods $p_n(\mathbf{x}|f_{\text{NL}})$ and $p_s(\mathbf{x}|f_{\text{NL}})$:

$$D_{n,s} = \int df_{\text{NL}} p_n(\mathbf{x}|f_{\text{NL}}) \log \frac{p_n(\mathbf{x}|f_{\text{NL}})}{p_s(\mathbf{x}|f_{\text{NL}})}, \quad (15)$$

where $p_n(\mathbf{x}|f_{\text{NL}})$ and $p_s(\mathbf{x}|f_{\text{NL}})$ are the likelihoods for the *Northern* and the *Southern hemispheres*, respectively. Actually, we use the symmetrized statistic D , defined as:

$$D = \frac{1}{2} (D_{n,s} + D_{s,n}). \quad (16)$$

We have found that the distance D for the likelihood distributions of the f_{NL} parameter estimated in the *Northern* and the *Southern hemispheres* defined by the dipolar pattern described by Hoftuft et al. (2009) is much larger than it would be expected from Gaussian and isotropic random CMB simulations. In particular, such a distance has a p-value ≈ 0.04 . This result is a further evidence on the largely discussed WMAP North-South asymmetry, and it is as well an indication that such asymmetry is manifested in terms of the non-Gaussianity of the CMB temperature fluctuations, in agreement with previous results (e.g., Park 2004; Hansen et al. 2004b; Eriksen et al. 2004b; Vielva et al. 2004; Cruz et al. 2005; Eriksen et al. 2005; Land & Magueijo 2005; Monteserín et al. 2008; Råth et al. 2009; Rossmanith et al. 2009).

At this point, it is worth recalling that the analysis described above has been performed assuming isotropy, i.e., we have used the same type of correlations to described the second-order statistics in both the *Northern* and in the *Southern hemispheres*. However, the result obtained by Hoftuft et al. (2009) indicates that these two hemisphere might be described by two different correlations (i.e., the sky would not be isotropic any longer). The dipolar modulation proposed by Hoftuft et al. (2009) was small (its amplitude was lower than 0.7%), but significant (a 3.3σ detection was claimed). Assuming this point, we have repeated our previous analysis, but using different statistical properties for the correlation matrices in the two halves. The way we have estimated these new correlation matrices is as follows: we have generated 500,000 simulations (in the same way it has been already described at the beginning of Section 4, and, once the co-added maps are degraded to NSIDE=32, each one of the simulations have been modified by applying the dipolar modulation estimated by Hoftuft et al. (2009) from the WMAP data. It is from these modulated simulations that we have estimated the new correlation matrices needed to estimate the likelihood probabilities. The result of this test is presented in figure 8. The conclusions related to the f_{NL}

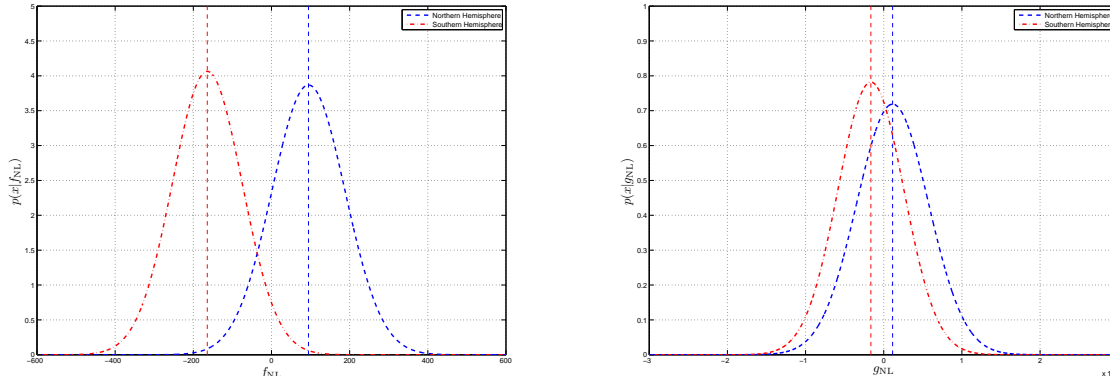


Figure 7. The left panel present the likelihood on f_{NL} obtained from a pure *quadratic* analysis $-p(\mathbf{x}|f_{\text{NL}})$ —, whereas the right plot provides the likelihood on g_{NL} from a pure *cubic* study $-p(\mathbf{x}|g_{\text{NL}})$. Dashed lines correspond to the *Northern hemisphere*, whereas dot-dashed lines are for the *Southern* half. Vertical lines indicate the maximum likelihood estimation of the non-linear coupling parameters: \hat{f}_{NL} and \hat{g}_{NL} .

estimation are essentially the same: on the one hand the analysis of the *Northern hemisphere* provides a constraint compatible with the Gaussian scenario, whereas the *Southern hemisphere* is not; on the other hand, the distance between both distributions is again too large (it also has a p-value –as compared to, in this case, anisotropic simulations– increases up to ≈ 0.09 (estimated in terms of the KLD). However, despite this slight change in the f_{NL} hemispherical estimation, dramatic differences can be observed for the pure *cubic* scenario. Interestingly, accounting for the dipolar modulation correction reveals an extra departure from anisotropy related to the g_{NL} constraints. The dipolar modulation makes the maximum likelihood estimation of g_{NL} highly incompatible between both hemispheres. In particular, the distance between both distributions is extremely rare as compared with the expected behaviour from Gaussian and anisotropic CMB simulations (generated, as explained above, by applying the dipolar modulation reported by Hoftuft et al. (2009)): it has a p-value of ≈ 0.002 , in the sense of the KLD.

We have also studied whether a WMAP data corrected by the dipolar modulation found by Hoftuft et al. (2009) could present a behaviour compatible with the Gaussian and isotropic hypotheses. Results for the corrected WMAP data are given in figure 9. Notice that we do not see any significant differences from the previous situation (i.e., the case in which uncorrected WMAP data was analyzed assuming anisotropy): the dipolar modulation does not affect to the f_{NL} and g_{NL} constraints.

Summarizing, the results obtained in this subsection seem to confirm that there is some kind of anomaly related to an hemispherical asymmetry as the one defined by the dipolar pattern reported by Hoftuft et al. (2009), in the sense of the f_{NL} parameter. Even more, when WMAP data is analyzed using correlations compatible with the dipolar modulation suggested by Hoftuft et al. (2009), not only asymmetries related to the f_{NL} parameter are clear, but also associated to the *cubic term* (i.e., the g_{NL} parameter). Intriguingly, the correction of the WMAP data in terms of this dipolar modulation is not enough to obtain a CMB signal compatible with a Gaussian and isotropic random field.

At this point, it is worth mentioning that the dipolar modulation of Hoftuft et al. (2009) was obtained by considering second-order moments of the CMB data and, therefore, this correction only addresses the problems related to an asymmetry in terms of this order. Hence, it is not totally surprising that this dipolar modulation correction is not sufficiently satisfactory to solve the anomaly reported in this work, since such anomaly is related to higher-order moments. It is also need to point out that we have tested that the dipolar modulation correction of the WMAP data does not affect the results obtained from an all-sky analysis of the CMB data.

Finally, let us recall that, in a recent work, Rudjord et al. (2009) searched for specific asymmetries related to the local estimation of the f_{NL} parameter, by using needlets. Contrarily to our findings, in this work no significant asymmetry was found when analyzing WMAP data. There are some differences between the analyses that could explain the discrepancy, although they have to be taken as mere suggestions. First, the kind of non-Gaussianity that is probed by each work is different: whereas the Rudjord et al. (2009) paper explore a f_{NL} model that is local in the gravitational potential (from which the non-Gaussian temperature fluctuations are obtained taking into account all the gravitational effects), here we adopt a local model in the Sachs-Wolfe regime. Second, they work at the best WMAP resolution (around 10-20 arcmins), whereas we focus on scales of around 2° . Third, we explore an specific division of the sky (the one reported by Hoftuft et al. (2009)), whereas they consider several divisions that, not necessarily, have to match the one used by us (they explore hemispherical divisions within an interval of around 30°).

5 CONCLUSIONS

We have presented an extension of our previous work (Vielva & Sanz 2009), by defining a parametric non-Gaussian model for the CMB temperature fluctuations. The non-Gaussian model is a local perturbation of the standard CMB Gaussian field, which (under certain circumstances) is related to

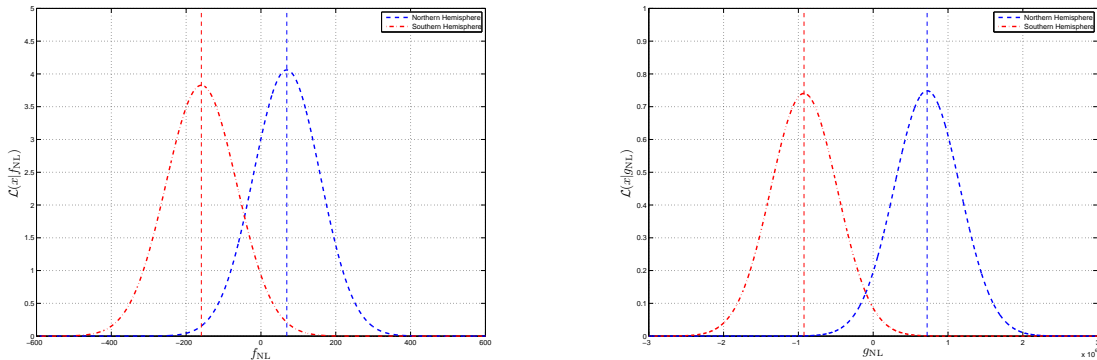


Figure 8. As in figure 7, but for the case in which the WMAP data has been analyzed using correlation matrices that account for the dipolar modulation.

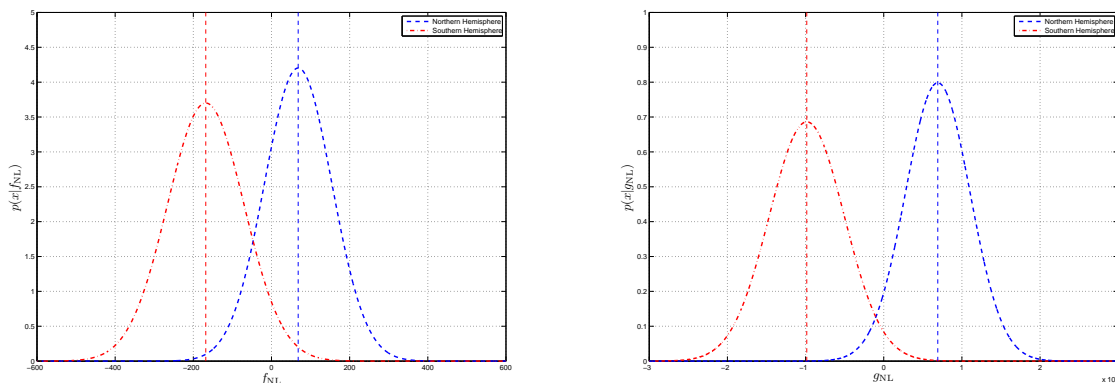


Figure 9. As in figure 7, but for the case in which the WMAP data has been corrected by the dipolar modulation.

an approximative form of the weak non-linear coupling inflationary model at scales larger than the horizon scale at the recombination time (i.e., above the degree scale, see for instance Komatsu et al. 2001; Liguori et al. 2003). For this model, we are able to build the posterior probability of the data given the non-linear parameters f_{NL} and g_{NL} . From these pdfs, optimal maximum likelihood estimators of these parameters can be obtained.

We have verified with WMAP-like simulations that the maximum likelihood estimation of the *quadratic* non-linear coupling parameters (\hat{f}_{NL}) is unbiased, at least for a reasonable range of values, even when non-Gaussian simulations also account for a *cubic* term. In particular, we found that for simulated non-Gaussian coefficients such as $|\hat{f}_{\text{NL}}| \lesssim 400$ and $|\hat{g}_{\text{NL}}| \lesssim 5 \times 10^5$, the estimation of f_{NL} is accurate and efficient. However, when trying to study the case in which only a pure *cubic* model is addressed, the situation is different. In particular, the simulated *quadratic* term has an important impact on the estimation of g_{NL} . For instance, if a pure *quadratic* non-Gaussian model is simulated with a value of $\hat{f}_{\text{NL}} \equiv 400$, a value of $\hat{g}_{\text{NL}} \approx 2.5 \times 10^5$ is wrongly estimated. This results indicates, obviously, that the *quadratic* term is more important than the *cubic* one in the expansion of the local non-Gaussian model, and, therefore, that not accounting properly for the former might have a dramatic

impact on the latter. Contrarily, the opposite situation is much more unlikely. Finally, we have investigated the joint estimation of the f_{NL} and g_{NL} parameters. In this case we find that for a similar regime as the one mentioned above (i.e., $|\hat{f}_{\text{NL}}| \lesssim 400$ and $|\hat{g}_{\text{NL}}| \lesssim 5 \times 10^5$), an accurate and efficient estimation of the non-linear coupling parameters is obtained. However, for larger values of these coefficients, we find that the parameter estimation is highly biased, favouring a region of the parameter space of larger values for both coefficients.

We have addressed, afterwards, the analysis of the WMAP 5-year data. We have consider two different analyses. First, we have investigated the case of an all-sky analysis (except for the Galactic area not allowed by the WMAP KQ75 mask). Second, and motivated by previous findings, we have performed a separated analysis of two hemispheres. In particular, the hemispherical division associated to the dipolar pattern found by Hoftuft et al. (2009) was considered.

Regarding the all-sky analysis, we find, for the case in which a pure *quadratic* model is investigated, the same result that we already found in our previous work (Vielva & Sanz 2009). In particular, we determine that $-154 < f_{\text{NL}} < 94$ at 95%. Equivalently, for the case of a pure *cubic* non-Gaussian model we establish $-5.6 \times 10^5 < g_{\text{NL}} < 6.4 \times 10^5$ at 95%. This

is in agreement with a recent work by Desjacques & Seljak (2009), where an analysis of LSS data was performed. The result that we provide in this paper is, as far as we know, the first direct constraint on g_{NL} from CMB data alone. Finally, we have also investigated the case of a joint estimation of the *quadratic* and *cubic* non-linear coupling parameters. In this case, the constraints obtained on f_{NL} and g_{NL} are virtually the same as the ones already reported for the independent analyses.

We have performed a model selection to evaluate which of the four hypotheses (i.e. Gaussianity, a pure *quadratic* model, a pure *cubic* model and a general non-Gaussian scenario) is more likely. Since a well motivated prior for the non-linear coupling parameters is lacking, we have used asymptotic model selection criteria (like AIC and BIC), instead of more powerful Bayesian approaches, like the Bayesian Evidence or the posterior ratio test. Both methodologies (AIC and BIC) indicates that the Gaussian hypothesis is more likely than any of the non-Gaussian models. We also found that, among the non-Gaussian scenarios, the one with a pure *quadratic* model is the most favoured one, whereas the general one (i.e. $f_{\text{NL}} \neq 0$ and $g_{\text{NL}} \neq 0$) is the most unlikely.

The analysis of the WMAP data in two hemispheres revealed that, whereas both halves of the sky present similar constraints on the g_{NL} parameter (and, in both cases, not indicating any significant incompatibility with the zero value), the analysis of a pure *quadratic* scenario showed a clear asymmetry. First, the f_{NL} value in the hemisphere whose pole is closer to the Southern Ecliptic Pole, is $\hat{f}_{\text{NL}} = -164 \pm 62$. Which implies that $f_{\text{NL}} < 0$ at 96%. Even more, the distance between both likelihoods (given in terms of the KLD) presents a p-value of ≈ 0.04 .

We have also analyzed the WMAP data after by considering different correlation properties in each hemisphere (according to the dipolar modulation described by Hoftuft et al. (2009)). We have tested that the behaviour found for the f_{NL} is practically the same as before, and that, in addition, an extra anomaly appears associated with the g_{NL} parameter. In particular, the distance between both likelihoods is anomalously large as well (it corresponds to a p-value of $\lesssim 0.002$). Further test was performed after correcting WMAP data from the dipolar modulation. In this case the asymmetries in the maximum-likelihood estimations of both non-linear coupling parameters remain unaltered. Hence, these results indicate that, as it has been previously reported in other works, there are evidences of anisotropy in the WMAP data, reflected as an asymmetry between two opposite hemispheres. Such anomaly is related to a different distribution for a non-linear coupling parameter related to the *quadratic* term. However, a correction in terms of a dipolar modulation as the one proposed by Hoftuft et al. (2009), seems not to be sufficient to account for this anomaly related to the likelihood distribution of the f_{NL} parameter.

ACKNOWLEDGEMENTS

We thank Belén Barreiro and Enrique Martínez-González for useful comments. We acknowledge partial financial support from the Spanish Ministerio de Ciencia e Innovación project AYA2007-68058-C03-02. PV also thanks financial support from the *Ramón y Cajal* programme. The authors

acknowledge the computer resources, technical expertise and assistance provided by the Spanish Supercomputing Network (RES) node at Universidad de Cantabria. We acknowledge the use of Legacy Archive for Microwave Background Data Analysis (LAMBDA). Support for it is provided by the NASA Office of Space Science. The HEALPix package was used throughout the data analysis (Górski et al. 2005).

REFERENCES

- Akaike H., 1973, in Petrov B.N., Czaki F., eds., Proc. 2nd International Symposium on Information Theory. Akad. Kiado, Budapest, p-267
- Barreiro R.B., 2009, in "Highlights of Spanish Astrophysics V", Proceedings of the VIII Scientific Meeting of the Spanish Astronomical Society (SEA) held in Santander, 7-11 July, 2008 (preprint arXiv:0906.0956)
- Bartolo N., Komatsu E., Matarrese S., Riotto A., 2004, Phys. Rep., 402, 103
- Cabella P., Liguori M., Hansen F.K., Marinucci D., Matarrese S., Moscardini L., Vittorio N., 2005, MNRAS, 358, 684
- Creminelli P., Senatore L., Zaldarriaga M., 2007, Journal of Cosmology and Astro-Particle Physics, 03, 005
- Cruz M., Martínez-González E., Vielva P., Cayón L., 2005, MNRAS, 356, 29
- Curto A., Aumont J., Macías-Pérez, Martínez-González E., Barreiro R.B., Santos D., Désert F.-X., Tristram M., 2007, A&A, 474, 23
- Curto A., Martínez-González E., Mukherjee P., Barreiro R.B., Hansen F.K., Liguori M., Matarrese S., 2008, MNRAS, 393, 615
- Curto A., Martínez-González E., Barreiro R.B., 2009, ApJ, 706, 399
- Desjacques V. & Seljak U., 2009, (preprint arXiv:0907.2257)
- Enqvist K. Takahashi T., 2008, Journal of Cosmology and Astro-Particle Physics, 09, 012
- Eriksen H.K., Hansen F.K., Banday A.J., Górski K.M., Lilje P.B., 2004a, ApJ, 605, 14
- Eriksen H.K., Novikov D.I., Lilje P.B., Banday A.J., Górski K.M., 2004b, ApJ, 612, 64
- Eriksen H.K., Banday A.J., Górski K.M., Lilje P.B., 2005, ApJ, 622, 58
- Gold B., 2009, ApJS, 130, 265
- Górski K.M., Hivon E., Banday A.J., Wandelt B.D., Hansen F.K., Reinecke M., Bartelmann M., 2005, ApJ, 622, 759
- Gott J.R., Colley W.N., Park C.-G., Park C., Mugnolo C., 2007, MNRAS, 377, 1668
- Gupta S. et al. (QUaD collaboration), 2009, ApJ, submitted, (preprint arXiv: arXiv:0909.1621)
- Hansen F.K., Cabella P., Marinucci D., Vittorio N., 2004a, ApJ, 607, L67
- Hansen F.K., Banday A. J., Górski K.M., 2004b, MNRAS, 354, 641
- Hikage C., Matsubara T., Coles P., Liguori M., Hansen F. K., Matarrese S., 2008, MNRAS, 389, 1439
- Hinshaw G. et al., 2009, ApJS, 130, 225
- Hoftuft J., Eriksen H.K., Banday A.J., Górski K.M., Hansen F.K. Lilje P.B., 2009, ApJ, 699, 9856

- Huang Q.-C., 2009, *Journal of Cosmology and Astro-Particle Physics*, 06, 035
- Land K., Magueijo J., 2005, *MNRAS*, 357, 994
- Komatsu E., Spergel D.N., 2001, *Phys. Rev. D*, 63, 063002
- Komatsu E., et al., 2003, *ApJS*, 148, 119
- Komatsu E., et al., 2009, *ApJS*, 180, 330
- Kullback S., Leibler R.A., 1951, *Ann. Math. Statist.*, 22, 79
- Liguori M., Matarrese S., Moscardini L., 2003, *ApJ*, 597, 57
- Liddle A., Lyth D. H., 2000, *Cosmological inflation and large-scale structure*, Cambridge University Press
- Monteserín C., Barreiro R.B., Vielva P., Martínez-González, Hobson, M.P., Lasenby A.N., 2008, *MNRAS*, 387, 209
- Mukherjee P., Wang Y., 2004, *ApJ*, 613, 51
- Park C.-G., 2004, *MNRAS*, 349, 313
- Pietrobon D., Cabella P., Balbi A., de Gasperis G., Vittorio N., *MNRAS*, 396, 1682
- Räth C., Morfill G.E., Rossmannith G., Banday A.J., Górski K.M., 2009, *PRL*, 102, 131301
- Rossmannith G., Räth C., Banday A.J., Morfill G.E., 2009, *MNRAS*, 399, 1921
- Rudjord O., Hansen F.K., Lan X., Liguori M., Marinucci D., Matarrese S., 2009, *ApJ*, 701, 369
- Sasaki M., Valiviita J., Wands J., 2006, *Phys. Rev. D*, 74, 103000
- Slozar A., Hirata C., Seljak U., Ho S., Padmanabhan N., 2008, *Journal of Cosmology and Astro-Particle Physics*, 08, 031
- Smith K.M., Senatore L., Zaldarriaga M., 2009, *JCAP*, 09,0006
- Spergel D.N. et al., 2007, *ApJS*, 170, 377
- Schwarz G., 1978, *Ann. Stat.*, 6, 461
- Vielva P., Martínez-González E., Barreiro R.B., Sanz J.L., Cayón L., 2004, *ApJ*, 609, 22
- Vielva P., Sanz J.L., 2009, *MNRAS*, 397, 837
- Yadav A.P.S., Wandelt B.D., 2008, *Phys. Rev. Lett.*, 100, 181301

APPENDIX A: N-PDF DERIVATION

In this Appendix we provide a detailed derivation of the N-pdf for the non-linear local model given by equation 5. As it has been already discussed, the objective is to make use of this likelihood to constrain the parameters that define the perturbative model. In particular, we are interested in estimating the parameters governing the *quadratic* (a) and *cubic* (b) terms, that, as it was explained in Section 2, can be related (under certain circumstances) to the non-linear coupling inflationary parameters f_{NL} and g_{NL} , respectively.

Let us recall here the expression for the N-pdf for the non-Gaussian model, as a function of the multinomial N-pdf ($p(\boldsymbol{\phi})$, equation 9):

$$p(\boldsymbol{x}|a, b) = p(\boldsymbol{\phi} = \boldsymbol{\phi}(\boldsymbol{x})) Z, \quad (\text{A1})$$

where Z is the determinant of the Jacobian of the $\boldsymbol{\phi} \rightarrow \boldsymbol{x}$ transformation (equation 10). For practical purposes (i.e., in order to constrain the non-linear coupling parameters) it is more convenient to deal with the log-likelihood $\mathcal{L}(\boldsymbol{x}|a, b)$

(given in equation 13), instead of $p(\boldsymbol{x}|a, b)$ (given in equation 9). Obviously, the later can be easily obtained by the inversion of equation 13.

Replacing equation 9 into equation 13, it is easy to show that the computation of $\mathcal{L}(\boldsymbol{x}|a, b)$ implies to solve two terms:

$$\mathcal{L}(x_i|a, b) = \log Z + \Omega, \quad (\text{A2})$$

where $\Omega \equiv \log \frac{p(\boldsymbol{\phi}=\boldsymbol{\phi}(\boldsymbol{x}))}{p(\boldsymbol{x}|0)}$, and, we recall it, $p(\boldsymbol{x}|0) \equiv p(\boldsymbol{\phi} = \boldsymbol{x})$.

Let us address the determination of these two terms ($\log Z$ and Ω) independently.

A1 Determination of the log-Jacobian

According to equation 10, the log-Jacobian for the $\boldsymbol{\phi} \rightarrow \boldsymbol{x}$ transformation is given by:

$$\log Z = \sum_{i=1}^N \log \left(\frac{\partial \phi_i}{\partial x_i} \right), \quad (\text{A3})$$

where ϕ_i as a function of x_i is given in equation 11. It is straightforward to prove that:

$$\frac{\partial \phi_i}{\partial x_i} = 1 + \sum_{m=1}^4 g_{m,i} \sigma^m, \quad (\text{A4})$$

where

$$\begin{aligned} g_{1,i} &= -2ax_i \\ g_{2,i} &= 3(2a^2 - b)x_i^2 - 2a^2 \\ g_{3,i} &= 20(-a^3 + ab)x_i^3 + 6(2a^3 - ab)x_i \\ g_{4,i} &= 5(14a^4 - 21a^2b + 3b^2)x_i^4 + 60(-a^4 + a^2b)x_i^2 \\ &\quad + 3(2a^4 - a^2b). \end{aligned} \quad (\text{A5})$$

Since we are considering a perturbative non-Gaussian model, then $\sum_{m=1}^4 g_{m,i} \sigma^m \ll 1$ and, therefore, the log-Jacobian can be easily derived from the Taylor expansion for the logarithm function:

$$\begin{aligned} \log Z &\approx \sum_{i=1}^N (g_{1,i}) \sigma + \left(g_{2,i} - \frac{1}{2} g_{1,i}^2 \right) \sigma^2 \\ &\quad + \left(g_{3,i} + \frac{1}{3} g_{1,i}^3 - g_{1,i} g_{2,i} \right) \sigma^3 \\ &\quad + \left(g_{4,i} - \frac{1}{2} g_{2,i}^2 + g_{1,i}^2 g_{2,i} - g_{1,i} g_{3,i} - \frac{1}{4} g_{1,i}^4 \right) \sigma^4. \end{aligned} \quad (\text{A6})$$

Taking into account that:

$$\begin{aligned} \frac{1}{N} \sum_{i=1}^N x_i^2 &= 1 + 2(a^2 + 3b)\sigma^2 + \mathcal{O}(\sigma^3) \\ \frac{1}{N} \sum_{i=1}^N x_i^3 &= 6a\sigma + \mathcal{O}(\sigma^3) \\ \frac{1}{N} \sum_{i=1}^N x_i^4 &= 3 + \mathcal{O}(\sigma^2), \end{aligned} \quad (\text{A7})$$

(as it can be trivially showed from equations 5 and 7) and replacing equation A5 into equation A6, one finally gets:

$$\frac{1}{N} \log Z \approx (2a^2 - 3b)\sigma^2 + \left(12a^4 - 36a^2b + \frac{27}{2} \right) \sigma^4, \quad (\text{A8})$$

up to the appropriate order in σ .

A2 Determination of Ω

Since we are dealing with a perturbative model (i.e., $\phi = \mathbf{x} + \boldsymbol{\epsilon}$, with $\boldsymbol{\epsilon} \ll \mathbf{x}$ and where $\boldsymbol{\epsilon} \equiv \boldsymbol{\eta}\sigma + \boldsymbol{\nu}\sigma^2 + \boldsymbol{\mu}\sigma^3 + \boldsymbol{\lambda}\sigma^4$, according to equation 11) it is interesting to notice that the probability function $p(\phi = \phi(\mathbf{x}))$ can be expanded in terms of the Taylor expansion, up to the appropriate order:

$$p(\phi = \phi(\mathbf{x})) = P + \epsilon^i \partial_i P + \frac{1}{2} \epsilon^i \epsilon^j \partial_{ij} P + \frac{1}{6} \epsilon^i \epsilon^j \epsilon^k \partial_{ijk} P + \frac{1}{24} \epsilon^i \epsilon^j \epsilon^k \epsilon^l \partial_{ijkl} P + \mathcal{O}(5), \quad (\text{A9})$$

where, for simplicity, we define $P \equiv p(\phi = \mathbf{x} + 0) \equiv p(\mathbf{x}|0)$. The function $\partial_i Y(\mathbf{x})$ is the derivative of $Y(\mathbf{x})$ with respect to x_i , i.e.: $\partial_i Y(\mathbf{x}) \equiv \frac{\partial Y(\mathbf{x})}{\partial x_i}$. Equivalently, $\partial_{ij} Y(\mathbf{x}) \equiv \frac{\partial}{\partial x_j} \partial_i Y(\mathbf{x})$, $\partial_{ijk} Y(\mathbf{x}) \equiv \frac{\partial}{\partial x_k} \partial_{ij} Y(\mathbf{x})$, and $\partial_{ijkl} Y(\mathbf{x}) \equiv \frac{\partial}{\partial x_l} \partial_{ijk} Y(\mathbf{x})$.

Taking into account this expansion, we have::

$$\frac{p(\phi = \phi(\mathbf{x}))}{p(\mathbf{x}|0)} = 1 + A^i \epsilon_i + \frac{1}{2} A^{ij} \epsilon^i \epsilon^j + \frac{1}{6} A^{ijk} \epsilon^i \epsilon^j \epsilon^k + \frac{1}{24} A^{ijkl} \epsilon^i \epsilon^j \epsilon^k \epsilon^l, \quad (\text{A10})$$

where, $A^i \equiv \frac{\partial_i P}{P}$, $A^{ij} \equiv \frac{\partial_{ij} P}{P}$, $A^{ijk} \equiv \frac{\partial_{ijk} P}{P}$, and $A^{ijkl} \equiv \frac{\partial_{ijkl} P}{P}$. It is trivial to show that these quantities are related to the data \mathbf{x} , its expected correlation $\boldsymbol{\xi} = [\xi_{ij}]$, and the model (i.e., a and b). After some algebra, one trivially finds:

$$\begin{aligned} A_i &= -\xi_{ij}^{-1} x^j, \\ A_{ij} &= -\xi_{ij}^{-1} + A_i A_j, \\ A_{ijk} &= A_{ij} A_k - A_j \xi_{ik}^{-1} - A_i \xi_{jk}^{-1} \\ A_{ijkl} &= A_i A_j A_k A_l + \xi_{ij}^{-1} \xi_{kl}^{-1} + \xi_{ik}^{-1} \xi_{jl}^{-1} + \xi_{jk}^{-1} \xi_{il}^{-1} \\ &\quad - A_k A_l \xi_{ij}^{-1} - A_j A_l \xi_{ik}^{-1} - A_i A_l \xi_{jk}^{-1} \\ &\quad - A_k A_i \xi_{jl}^{-1} - A_k A_j \xi_{il}^{-1} - A_i A_j \xi_{kl}^{-1}. \end{aligned} \quad (\text{A11})$$

Since we are interested in the quantity $\log \frac{p(\phi=\phi(\mathbf{x}))}{p(\mathbf{x}|0)}$, the logarithm function can be expanded up to the appropriate order. It is straightforward to obtain:

$$\Omega = F\sigma + G\sigma^2 + H\sigma^3 + I\sigma^4 + \mathcal{O}(5), \quad (\text{A12})$$

where:

$$\begin{aligned} F &= -\frac{1}{N} (S_{\boldsymbol{\eta}\mathbf{x}}), \\ G &= -\frac{1}{N} \left(S_{\boldsymbol{\nu}\mathbf{x}} + \frac{1}{2} S_{\boldsymbol{\eta}\boldsymbol{\eta}} \right), \\ H &= -\frac{1}{N} (S_{\boldsymbol{\lambda}\mathbf{x}} + S_{\boldsymbol{\eta}\boldsymbol{\nu}}), \\ I &= -\frac{1}{N} \left(S_{\boldsymbol{\mu}\mathbf{x}} + S_{\boldsymbol{\lambda}\boldsymbol{\eta}} + \frac{1}{2} S_{\boldsymbol{\nu}\boldsymbol{\nu}} \right). \end{aligned} \quad (\text{A13})$$

We have defined the operator $S_{\alpha\beta} \equiv \alpha^i \xi_{ij}^{-1} \beta^j$, and $\boldsymbol{\eta}$, $\boldsymbol{\nu}$, $\boldsymbol{\lambda}$ and $\boldsymbol{\mu}$ where defined in equation 12.

Therefore, taking into account equations A8 and A12, the final expression for the log-likelihood $\mathcal{L}(\mathbf{x}|a, b)$ is:

$$\begin{aligned} \frac{1}{N} \mathcal{L}(\mathbf{x}|a, b) &= F\sigma + (2a^2 - 3b + G)\sigma^2 + H\sigma^3 \\ &\quad + \left(12a^4 - 36a^2b + \frac{27}{2}b^2 + I \right) \sigma^4. \end{aligned} \quad (\text{A14})$$